Computation of the Peierls stress in tantalum with an extended-range modified embedded atom method potential

2005 J. Phys.: Condens. Matter 17 2003

(http://iopscience.iop.org/0953-8984/17/12/022)

INSTITUTE OF PHYSICS PUBLISHING JOURNAL OF PHYSICS: CONDENSED MATTER

J. Phys.: Condens. Matter **17** (2005) 2003–2018 doi:10.1088/0953-8984/17/12/022

Computation of the Peierls stress in tantalum with an extended-range modified embedded atom method potential

Pierre-Matthieu Anglade, Gérald Jomard, Gregory Robert and Gilles Zérah

Département de Physique Théorique et Appliquée, Service de Physique de la Matière Condensée, CEA/DAM Bruyères le Châtel, France

E-mail: gilles.zerah@cea.fr

Received 3 September 2004, in final form 6 January 2005
Published 11 March 2005
Online at stacks.iop.org/JPhysCM/17/2003

Abstract

When computing the Peierls stress of screw dislocations in tantalum by means of classical molecular dynamics (CMD), we have observed that a suitable potential should be able to reproduce the complicated angular dependence of forces arising in the core structure of dislocations. This prevents the use of simple embedded atom potentials, but we notice that more generally, effective interatomic potentials tend to overestimate the Peierls stress. Since the Peierls–Nabarro model of dislocation requires an accurate description of the generalized stacking fault (GSF) energy surface, we have decided to use the modified embedded atom method (MEAM) potential, which explicitly incorporates angular terms, whose coefficients are constrained to reproduce *ab initio* GSF data.

Calculations with our new tantalum empirical model show the importance of hard core screw dislocations and underline the problem of kinetics in Peierls stress calculations.

1. Introduction

As computing power continues to grow exponentially, classical molecular dynamics (CMD) simulations become more and more frequent. Among other applications like protein or other organic molecule simulations [1, 2], CMD is also used in simulations involving microstructures in metals, e.g. high energy cascades [3], or shocked material states [4, 5]. CMD simulations have also been used to address dislocations, from calculation of static properties such as the influence of shear stress in the 1970s [6], to studies of dynamical properties such as transitions between different dislocation motion mechanisms [7].

0953-8984/05/122003+16$30.00

Dislocations are the source of crystal plasticity, and therefore plastic properties depend strongly on them. While the long range properties of dislocations are well understood and described by means of elasticity, their core properties play a paramount role for quantities involving an interaction with the crystal lattice such as the Peierls stress and are still a topic of investigation. For exploring those properties, CMD is a tool of choice, provided that empirical potentials can be used to model accurately the distorted arrangement of atoms composing the dislocation core.

Considering the numerous successes of the embedded atom method (EAM) [8], and specifically the model proposed by Strachan *et al* in [9], we have initially chosen to use this model to simulate the Peierls stress of [111] screw dislocations and its evolution under pressure.

At zero pressure this potential yields a Peierls stress (τ_c) of about 800 MPa while experimental data [10] lead to an extrapolation to zero temperature of about 340 MPa [11]. We might guess that this is the consequence of the lack of angular terms in the EAM but other calculations using potentials which include angular terms result in similar values [12, 13]. To explain this discrepancy, it has been proposed [14, 15] that the Peierls stress measured in experiments does not correspond to uniform motion of a straight dislocation which is the geometry considered in these simulations.

Calculations with the modified generalized pseudopotential theory (MGPT) in [13], as well as *ab initio* simulations by Woodward and Rao [15], result in values for τ_c between 600 and 700 MPa. These results clearly strengthen the previously stated hypothesis. Meanwhile all those calculations rely on some approximations, and we decided to reconsider the problem with a somewhat different approach.

To this end, we have produced an empirical potential dedicated to this kind of calculation: that is to say, we have addressed this problem by including in the training set of our potential (that is, the set of quantities it will be fitted against) extensive information about the [110] GSF (generalized stacking fault) energy surface of tantalum. The potential then includes the ingredients of the Peierls–Nabarro model [16], and will one hopes yield a more accurate description of the Peierls stress.

The paper is organized as follows: in the first part we will briefly describe Peierls stress computation techniques; in the second part the formalism of the modified embedded atom method and the modification we have made to it will be described; then in the third part we will give the scheme of our fitting method; and finally in the last section we will discuss our results and conclude.

2. Peierls stress

The Peierls stress is known as the minimum stress required to move a straight dislocation irreversibly [13] in its glide plane. Since dislocations might move by thermally activated processes, adding that the Peierls stress is defined at 0 K [12] is commonly accepted.

Its value is most important because it governs plasticity thresholds; therefore it is used in mechanical models such as those of Khotari and Anand [17]. At zero temperature, crystals are homogeneous and uniform motion of dislocations might dominate under stress while other processes become more and more important with temperature. For example, in [7] Marian and co-workers show the first atomistic simulation evidence of the thermally activated double-kink process.

According to Schmid's law the Peierls stress should not depend on other components of the applied stress tensor. But BCC materials present some strong non-Schmid behaviour and τ_c depends on other matrix elements of the applied stress. Thus dislocations are not constrained

to slipping in the maximal resolved shear stress plane. Moreover, there are three kinds of slip directions for screw dislocations in BCC materials: one in planes of type [110] and two in planes of type [112], the so-called twinning and anti-twinning slips. Due to the construction of our MEAM potential (as will be explained later) we must restrict our study to slips in the direction $\langle 112 \rangle$. According to [13] this will result in a slightly overestimated Peierls stress compared to the one obtainable with twinning systems.

The nature of dislocations is not very compatible with the usual periodic conditions employed in molecular dynamics simulations. Indeed, a net Burgers vector is topologically incompatible with a fully periodic simulation cell.

Some solutions have been proposed to circumvent this problem:

- Use of a dipole or quadrupole of dislocations. This is the most straightforward solution. In an undisplaced multi-polar configuration of dislocations, interactions vanish by symmetry. But this is generally not true as soon as dislocations have moved: for large systems, this effect is small, and can be taken into account, since interactions between dislocations are accurately described by means of elasticity at long distances. This method also has the drawback of requiring twice or four times the atoms in the simulation cell compared with other methods to get a given dislocation density. Interactions between dislocations in periodic arrays are detailed in [18]. Quadrupolar areas are used for the calculation of τ_c in e.g. [12, 19].
- Implementation of Green function periodic boundaries [20]. The Green functions are employed to mimic the behaviour of the bulk crystal.
- Coupling of free boundaries in one direction with periodic boundaries in the others. This is a very efficient and attractive method. From the dislocation point of view it is not very different from a configuration in a multi-polar area. But for obvious reasons it cannot be used under pressure. This approach is used in [7].

Among those methods, we have chosen to use the quadrupolar area of dislocations with large simulation cells: this is the method where we think boundary condition effects are the smallest, and it can be checked by changing the cell's size. Indeed, we used cells of size 47×27 along axes [110] and [112], and a 123×71 box for results checking.

Having put dislocations in our simulation cell, it is now possible to estimate the Peierls stress: to this end, we apply step by step a pure shear strain to observe an irreversible dislocation displacement. The sample being wide and of cubic symmetry, this strain results in a pure shear stress. The latter—which generates the Peach–Kohler forces on the dislocation in the glide plane—is computed according to equation (1) where $\vec{n}$ is a normalized vector normal to the glide plane, $\vec{m}$ is the glide direction and $\underline{\underline{\sigma}}$ is the stress computed from the strain through equation (2):

$$\sigma_{\mathrm{rss}} = \vec{n} \cdot \underline{\underline{\sigma}} \cdot \vec{m} \tag{1}$$

$$\underline{\underline{\sigma}} = \underline{\underline{\underline{\underline{C}}}} \cdot \underline{\underline{\varepsilon}}. \tag{2}$$

Some inaccuracies occur because of long range interactions between dislocations. In [12] Segall *et al* evaluate them to be of the order of a tenth of a MPa for large circular free boundary cells. The periodic quadrupolar area of dislocations leads to smaller interaction effects with equivalent radii between dislocations. So the resulting inaccuracy from this effect in our simulations cells where the distances between dislocations are about 100 and 200 Å should be and is indeed small.

The choice of the strain step is crucial for accuracy: finite size effects result in a very small error bar due to the use of a more than 3×10^5 Å^2 checking cell. The Peierls stress is

calculated with the smallest strain which results in an irreversible dislocation displacement; the strain below this latter is about 5% smaller.

3. MEAM

Our goal is to build our own model for simulation of tantalum. Let us just consider two points. First, this metal is in a 3d electronic configuration; this implies that there are some short ranged, angular forces between atoms. This can be simply deduced merely by observation of the periodic table of the elements, where metals with unfilled d electronic states show much stronger elastic moduli and frequently non-close-packed structure. Second, we want to reproduce the properties of a localized defect: the dislocation cores. These localized defects are precisely the kinds of structures where angular and short range forces are expected to play an important role.

These two points led us to consider the MEAM formalism [21]. This choice is in agreement with the Li *et al* observations: they noted in [22] that forces in tantalum cannot be described accurately with a simple EAM potential.

3.1. Original formulation

In its initial formulation, the MEAM potential, like the EAM potential, can be described as the sum of a pair potential between atoms and a nonlinear function of the electronic density created on the site of a particular atom by all the surrounding atoms. At variance with the EAM formulation, in which the density created around a particular site depends only on the distance between atoms, the MEAM formalism introduces angular terms which are represented by Legendre polynomials. The MEAM has evolved throughout the years, from the late 1980s [23] to now. For instance, at the beginning, $\bar{\rho}$ (set of equations (6)) included angular terms up to order 2 only (equation (6*d*)). Later on, angular screening terms were added (set of equations (8)). Those terms, introduced in a somewhat ad hoc fashion, strongly limit the range of the pair interactions. Finally, some functions like $G(\Gamma)$ and f_c (equations (6*b*) and (7)) were given different analytical formulations. Because of such changes, to give an accurate view of the way in which MEAM is used here it is necessary to give a short reminder of the formalism which is fully explained in [23, 21, 26]. Then a brief summary of some functions is needed in order to emphasize and justify the changes we have made in order to get an accurate fitting of tantalum's properties.

The MEAM can actually be expressed in the following way:

$$E_i = F(\bar{\rho}_i) + \tfrac{1}{2}\sum_{j\neq i}\phi(|r_{ij}|) \times S_{ij} \times f_c(|r_{ij}|) \tag{3}$$

$$\phi(a) = \frac{2}{Z_1}\left\{U_{\text{Rose}}(a) - F[\bar{\rho}^0(a)]\right\} f_c(a) \tag{4}$$

$$F(\bar{\rho}) = AE_c\frac{\bar{\rho}}{\bar{\rho}^0}\ln\left(\frac{\bar{\rho}}{\bar{\rho}^0}\right) \tag{5}$$

$$\bar{\rho}_i = \bar{\rho}_i^{(0)} G(\Gamma_i) \tag{6a}$$

$$G(\Gamma_i) = \frac{2}{1+\mathrm{e}^{-\Gamma_i}} \tag{6b}$$

$$\Gamma_i = \sum_{l=1}^{3} t^{(l)}\left[\frac{\rho_i^{(l)}}{\rho_i^{(0)}}\right]^2 \tag{6c}$$

$$(\rho_i^{(l)})^2 = \sum_{j\neq i, k\neq (i,j)} \rho^{a(l)}(|r_{ij}|)\rho^{a(l)}(|r_{ik}|)P_l(\cos\theta_{kij})\frac{2^l l!}{\prod_{m=0}^{l-1} 2l-m} \tag{6d}$$

$$\rho^{a(l)}(r) = \mathrm{e}^{-\beta_l(\frac{r}{r_e}-1)} f_c(r) S_{ij} \tag{6e}$$

$$P_l(x) = \frac{1}{2^l l!}\frac{\mathrm{d}^l(x^2-1)^l}{\mathrm{d}x^l} \tag{6f}$$

$$f_c(x) = \begin{cases} 1 & x > 1 \\ \left[1-(1-x)^4\right]^2 & x \in [0,1] \\ 0 & x < 0 \end{cases} \tag{7}$$

$$S_{ij} = \prod_{k\neq i,j} S_{ikj} \tag{8a}$$

$$S_{ikj} = f_c\left[(C - C_{\min})(C_{\max} - C_{\min})\right] \tag{8b}$$

$$C = \frac{2(X_{ik}+X_{kj}) - (X_{ik}-X_{kj})^2 - 1}{1-(X_{ik}-X_{kj})^2} \tag{8c}$$

$$X_{ab} = (r_{ab}/r_{ij})^2. \tag{8d}$$

Equation (3) defines the energy of an atom i from the relative positions $\vec{r}_{ij}$ of its neighbours j. It looks basically the same as in the EAM: it relies on an embedding function F (equation (5)) depending on a density $\bar{\rho}$ and a pair interaction ϕ (equation (4)).

The pair interaction is defined in equation (4) so that in the reference crystal structure, the equation of states (EOS) is fully reproduced for a wide range of densities. Practically, it is a fit to an accurate EOS that is reproduced. In our case this fit is based on the formalism of Rose's universal equation of state for metals [24] (denoted as U_{Rose}) and the equation of state is computed *ab initio*. The variable a in equation (4) is the first-nearest-neighbour distance and $\bar{\rho}'^0(a)$ is the density on an atomic site in the reference crystal structure computed without use of the cut-off function.

Major changes from the EAM occur in two places:

- The EAM function ρ_i becomes $\bar{\rho}_i$ which instead of a linear superposition of scalar functions ρ_{ij} is dependent through the set of equations (6) upon four pair functions, $\rho^{a(0)}$, $\rho^{a(1)}$, $\rho^{a(2)}$ and $\rho^{a(3)}$, from the atoms in the neighbourhood. The subequation (6*d*) describes the angular terms included in $\bar{\rho}_i$ as a development in spherical harmonics with Legendre's polynomials (subequation (6*f*)). It depends on the angle between each pair of neighbouring atoms. (Note in subequation (6*d*) $\frac{0!}{0} = 1$.) This angular dependence of the density mimics the angular dependence of electronic shells s, p, d and f; yet it is only mimicking it. So the only common point is the angular dependence and the decaying shape. Introducing these functions, the goal is still to have a fast-evaluation potential. Thus they are taken into account in a very simple way—that is, through functions G (equation (6*b*)) and Γ (equation (6*c*)) and a set of tunable coefficients $t^{(l)}$. Those functions are chosen so that the angle dependent terms act as corrections on the radial density. And the strongest justification of the formalism of the equations of the set (6) is its ability to describe properties of metals which were not within reach of the EAM formalism.
- The three-body angular screening term S_{ij} is from the set of equations (8) where $C_{\min}$ and $C_{\max}$ are the two parameters of the screening. Indices i, j, a and b denote atomic sites. Note that in subequation (8*d*) the indices a and b stand for any combinations of i, j and k. To roughly depict effects of screening, let us draw an ellipse in a system with three atoms i, j and k, the first axis being $\vec{r}_j - \vec{r}_i$ and the other axis being of length $\sqrt{C}/2$ times

the length of the first one, where C is such that the ellipse passes through atom k. If C is lower than $C_{\min}$, interactions between i and j are totally screened by k; if it is between $C_{\min}$ and $C_{\max}$ they are partially screened; finally if C is larger than $C_{\max}$, no screening from atom k happens.

3.2. Modified formalism

This original formalism was used by Baskes to build first-nearest-neighbour (nn) potentials (e.g. [21]). Other potentials of the MEAM type have been developed in various ways by different authors (e.g. [25, 26]). For example Lee *et al* have developed a 2nd nn approach for BCC materials in [26]. Yet we found that forces are of somewhat longer range, exploring localized defects with DFT and the GGA for tantalum. An unrelaxed vacancy gives rise to forces stronger on the 2nd nn than on the 1st nn; even the 4th nn experience forces which are about a quarter of those on the 2nd nn. Planar faults also give rise to medium range forces whose significant extensions rely upon the surface indices. For example the forces extend[1] only to the third layer for surface faults in plane [112] and [111] while in plane [100] and [110] they extend over the fifth layer.

Let us consider the example of the unrelaxed vacancy as it is the most striking. In BCC materials there are 6 1st nn, 8 2nd nn, 12 3rd nn, 24 4th nn, 8 5th nn, ... According to our *ab initio* calculations, forces cannot be described with accuracy if one has a 1st nn potential. Indeed most of the forces (force modulus $\times$ number of atoms) resulting from the vacancy are on the longer range neighbours (3rd nn and 4th nn) due to their higher number and the low radial decrease of the forces.

So in order to get a better reproduction of *ab initio* data we had to increase our potential's effective radius and modify some details of the original formalism.

As in the original formalism, interactions are totally screened at short range in BCC structures, we have first introduced a parameter we called $\mathrm{Scr}_{\max}$ in order to allow longer range interactions to be taken into account. The function f_c in equation (8*b*) now becomes

$$f_c = [1 - (1 - x)^4]^4(1 - \mathrm{Scr}_{\max}) + \mathrm{Scr}_{\max}. \tag{9}$$

Instead of being from 1 (no screening) to zero (full screening), the screening function now ranges from 1 to $\mathrm{Scr}_{\max}$. The change in polynomial degree (from eight to sixteen) is due to continuity considerations: for example the elastic moduli are second derivatives of the energy and such a cut-off function allows the third derivative of the energy to be continuous. In the original formalism, the cut-off function was not supposed to effectively cut the interaction, since this task was already done by the angular screening. But as our angular screening gets weaker, we need to be more careful on this point.

Still out of concern for continuity, we changed equation (5), which now reads

$$F(x) = AE_c\frac{F_b(C_F x)}{C_F} \tag{10}$$

$$F_b(x) = \begin{cases} x\log(x) & \text{if } x > 1/\mathrm{e} \\ \frac{107}{6}\mathrm{e}^6x^7 - 63\mathrm{e}^5x^6 + \frac{153}{2}\mathrm{e}^4x^5 - \frac{97}{3}\mathrm{e}^3x^4 & \text{if } x \leqslant 1/\mathrm{e}. \end{cases} \tag{11}$$

The polynomial was chosen so that first, second and third derivatives of F tend to zero when the density tends to zero and are continuous over the range $]0, +\infty[$.

Finally the computation of ϕ from Rose's universal equation of state for metals and the electron density in the reference structure gets a little more tricky. It still relies on the Chen–

[1] They are in modulus over 10% of the maximum force.

Möbius formulae [27] as in Lee's article for 2nd nn MEAM [26]. But the expression is now the following:

$$\phi(R) = \psi(R) + \sum_{i=1} \frac{\prod_{j=2}^{N} Z'^{k_j}_j}{(-Z_1)^i} \psi \left(R \prod_{j=2}^{N} r_{1j}^{k_j} \right) \frac{i!}{\prod_{j=2}^{N} k_j!} \tag{12}$$

where $\sum k_j = i$ and $k_j \in [0, i]$; Z_1 is the coordination number for 1st nn; Z'_i is the corrected coordination number for the ith nn—the correction occurs because of angular screening; and $\psi(R)$ is just $\frac{2}{Z_1}\{U_{\text{Rose}}(R) - F[\bar{\rho}^0(R)]\}$.

If the partial densities and the EOS are zero beyond a given radius, then convergence is certain. Therefore we compute this with all densities and the EOS being cut, so that they yield zero values for distances larger than a specified cut radius, which is another difference from the original formalism where equation (4) is computed without use of a cut-off function.

4. Fitting the potential

As noticed previously, the Peierls–Nabarro model describes dislocation mobility on the basis of the full generalized stacking fault (GSF) energy surface [28, 29]—also known as the gamma surface—in the glide plane. In BCC metals the most important surface is the [110] for two reasons. First, one observes glides in directions [110], [112] and [123] which are all combinations of a few glides in the set of directions $\{110\}$ (e.g. $[123] = 2 \times [011] + [101]$). Second, of those three directions, it has the lowest indices and it is the closest packed plane; the Schmid and Boas observations [30] led them to conclude that plastic flow occurs during the sliding of such planes across one another, so it should be the glide plane.

To our knowledge, unlike specific points called stable stacking fault energies—e.g. the well known ABCABABC in FCC crystals—the full shape of a Γ-surface cannot be measured experimentally. Thus it is necessary to rely on *ab initio* calculations. We have decided to rely only on such data for our fit. This is acceptable as, for tantalum, *ab initio* calculations give a very good agreement with experiment for many data: EOS, phonons, equilibrium volumes [31], ...

As the [110] Γ-surface obviously involves all the parameters of a MEAM because of symmetry breaking, we have adjusted all the parameters of our model simultaneously.

The equation of state of tantalum has been computed with two methods, which have distinct qualities.

The most accurate but also the most computer intensive is a full-potential version of the linear augmented plane wave method (FP-LAPW) [32]. The self-consistent calculations are performed with a fully relativistic treatment including spin–orbit coupling for the valence states (5s, 6s, 5d, 5p and 4f). The lattice is divided into non-overlapping muffin-tin spheres with a radius R_{mt} and an interstitial region. In order to be able to reach very high pressure the volumes occupied by the spheres are kept constant (50% volume). Inside the muffin-tin spheres the basis functions are expanded in spherical harmonics up to order $l = 10$. In the interstitial region the basis functions are expanded into plane waves and the plane wave cut-off k_{max} is fixed as $k_{\text{max}} R_{\text{mt}} = 10$. Finally we used 72 k-points in the irreducible Brillouin zone and the generalized gradient approximation, GGA, as implemented in [33].

The second method using pseudopotentials that enables efficient calculations was carried out with Abinit [34, 35]. The pseudopotential used has 13 valence electrons with an energy cut-off of 60 Hartree and the HGH [36] formalism. The reciprocal space sampling was performed with an optimized k-point grid corresponding to 240 k-points in the irreducible Brillouin zone. Generalized gradient corrections are added in the form of the Perdew–Burke–Ernzerhof GGA [37].

Table 1. Parameters for the EOS used in our MEAM potential for tantalum.

Rose's parameters (13)	
E_0	-8.09 eV
r_e	2.861 Å
α	4.856
δ	0.0374
ε	-0.0284
Polynomial	
$\sum_{i=0}^{6} A_i \times r^i$ (r^i in Å, $r \in [2.861, 5.5]$)	
A_0	$1.118\,961\,950\,422\,440 \times 10^{+3}$
A_1	$-1.572\,662\,889\,147\,018 \times 10^{+3}$
A_2	$9.007\,365\,924\,422\,019 \times 10^{+2}$
A_3	$-2.725\,527\,619\,862\,307 \times 10^{+2}$
A_4	$4.618\,945\,202\,635\,572 \times 10^{+1}$
A_5	$-4.162\,506\,237\,125\,867 \times 10^{+0}$
A_6	$1.557\,903\,195\,730\,858 \times 10^{-1}$

Results from these two methods are very close to one another and to experimental ones in the compression part of the EOS. We have fitted the data with a slightly modified Rose universal formula for metal equations of state [24] (equation (13)). Numerical values are displayed in the first part of table 1.

$$U_{\text{Rose}} = E_0(1 + a^* + \delta a^{*3} + \varepsilon a^{*4})\mathrm{e}^{-a^*} \tag{13}$$

where a^* is $\alpha(r/r_e - 1)$. The polynomial coefficients are those used to cut the EOS to ensure convergence of formula (12) at the cut radius r_{cut}. Their values are useful only in the range [2.861, 5.5] Å.

Elastic moduli are calculated using Abinit and formulations proposed by Beckstein (in his 'Elastic Constant How-to' from [38]) and Mehl (in [39]) for cubic materials:

$$E = E_0 + V_0 \sum_{i=1}^{6} \left(\sigma_i e_i + \tfrac{1}{2} \sum_{j=1}^{6} C_{ij} e_i e_j \right). \tag{14}$$

Equation (14) is Taylor's development to the second order of a solid energy towards homogeneous deformations e_i. As shown in equation (16), the elements of deformation are part of the matrix $\underline{\underline{\varepsilon}}$. This matrix is applied to each vector $\vec{r}$ of the solids; these become $\vec{r}'$. The indices are chosen according to Voigt's notation.

$$\vec{r}' = (\underline{\underline{I}} + \underline{\underline{\varepsilon}})\vec{r} \tag{15}$$

$$\varepsilon = \begin{pmatrix} e_1 & \frac{1}{2}e_6 & \frac{1}{2}e_5 \\ \frac{1}{2}e_6 & e_2 & \frac{1}{2}e_4 \\ \frac{1}{2}e_5 & \frac{1}{2}e_4 & e_3 \end{pmatrix}. \tag{16}$$

The Abinit calculations still use the same settings and are carefully converged. The strains presented in table 2 for C' and C_{44} are symmetric with respect to γ. Thus they require fewer calculations for the same level of accuracy.

For each pressure, to compute B (the bulk modulus) we used seven values of γ ranging in $[-0.006; 0.006]$, while we needed only four values of γ ranging in $[0.000; 0.018]$ to get C' and between 0.000 and 0.009 for the shear modulus C_{44}.

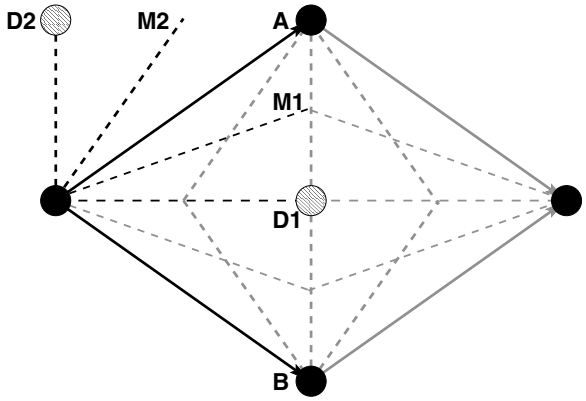

Figure 1. BCC unit cell based on axis [110], A $= \left[\frac{\bar{1}}{2}\frac{1}{2}\frac{1}{2}\right]$ and B $= \left[\frac{\bar{1}}{2}\frac{1}{2}\frac{\bar{1}}{2}\right]$. Plain black circles are atoms of height zero and hashed ones are atoms of height one half of [110]. Grey lines are equivalent to appropriate black ones due to crystal symmetries.

Table 2. Deformations used to compute elastic moduli of tantalum.

Parameters	$\Delta E/V$
$e_1 = -e_2 = \gamma, e_3 = (1-\gamma^2)^{-1} - 1$	$2C'\gamma^2 = (C_{11} - C_{12})\gamma^2$
$e_1 = e_3 = e_3 = \gamma$	$\frac{9}{2}B\gamma^2 = \frac{3}{2}(C_{11} + 2C_{12})\gamma^2$
$e_6 = \gamma, e_3 = \gamma^2(4-\gamma^2)^{-1}$	$\frac{1}{2}C_{44}\gamma^2$

The [110] Γ-surface evaluation was the longest part of the computations. Let us give a brief reminder about the GSF. Suppose that we cut an infinite crystal along a plane. Then we put the two parts together but with one slightly moved towards the other by a vector $\vec{v}$. Meanwhile the atoms have not moved at all. It is clear that when $\vec{v}$ is a lattice vector the energy is unchanged. For all other values we get an energy difference per surface unit which is periodic in the cut plane. This is the unrelaxed generalized stacking fault energy surface. The adjective 'generalized' comes from the fact that it is defined even when it is unstable.

If we let the atoms move freely, they relax totally so that we have very few energy levels on exploring the complete surface—only the perfect crystal and the eventual stable stacking fault energies. That is why the so-called relaxed GSF is obtained when atoms can move only along the axis perpendicular to the surface.

The smallest unit cell whose a axis is [110] and for which b and c are perpendicular to a is drawn in figure 1. It has two atoms in two layers along axis [110].

Calculating relaxed GSF energies requires one to assume that energy is localized near the plane. Our calculation in the GGA shows that using six, eight or ten layers of atoms in the plane [110] leads to equivalent results. Thus we were confident using a six-layer cell.

As the calculations are very time-consuming, we have done them only for a few points in a few directions along some axes shown in black in figure 1. These axes are denoted as D1, M1, A, M2 and D2. As shown in figure 1 this provides an accurate sampling of the GSF because of the unit cell symmetries.

In our calculation of the relaxed GSF, forces are minimized until they all are under 10^{-3} Hartree/b.

Table 3. MEAM 4th nn parameters.

Cut parameters	
Δ_r (Å)	3.56
r_{cut} (Å)	5.50
Embedding	
A	0.116 344 9805
C_F	1.047 847 864
Screening	
C_{min}	$1.051\,88 \times 10^{-6}$
C_{max}	2.362 574 499
Scr_{max}	0.465 322 6474
Partial densities	
β_0	5.766 908 954
β_1	1.427 893 495
β_2	3.848 857 747
β_3	8.761 198 815
t_1	−102.499 504 6
t_2	−76.164 261 15
t_3	3.407 165 574

4.1. Parameters of the potential

Using the data described above, we have used a Powell routine coupled with a random starting point generator to find a set of parameters able to minimize a cost function defined as (17).

$$Q = \sum \left(\alpha \frac{|V - V_{\text{t}}|}{\max(|V_{\text{t}}|, \text{tol.})} \right)^E \tag{17}$$

where the V are energy differences or values of elastic moduli computed with the current parameters of the MEAM, V_{t} are the theoretical values computed with Abinit and tol., E and α are parameters describing the relative importance of the V.

This results in a potential described by the parameters displayed in table 3.

Some of those parameters have rather classical values for MEAM potentials (e.g. C_{max}, $A \ldots$). Some others like t_1 and t_2 will lead to rather drastic effects. They are indeed about two orders of magnitude higher than the usual values in first-nearest-neighbour and second-nearest-neighbour MEAM potentials.

4.2. Quality of the fit

We have done the fitting job on more than a hundred points. Thus it is not easy to draw an exhaustive and still comprehensible figure showing the result. Nevertheless figure 2 gives an accurate and representative sample: two lines of the [110] GSF at three different pressures.

Most of the data from the potential are in fairly good agreement with their fitting counterparts at low pressure. However, even there, some features are not reproduced by the 4th nn MEAM. For example, along direction D1, the energy is overestimated around the middle of the curve; and this tendency keeps increasing when pressure is growing. Discrepancies increase with pressure, as can be easily seen in figure 2. At 120 GPa, one can state that the GSF energy surface of our 4th nn MEAM and that of the *ab initio* calculation are significantly different.

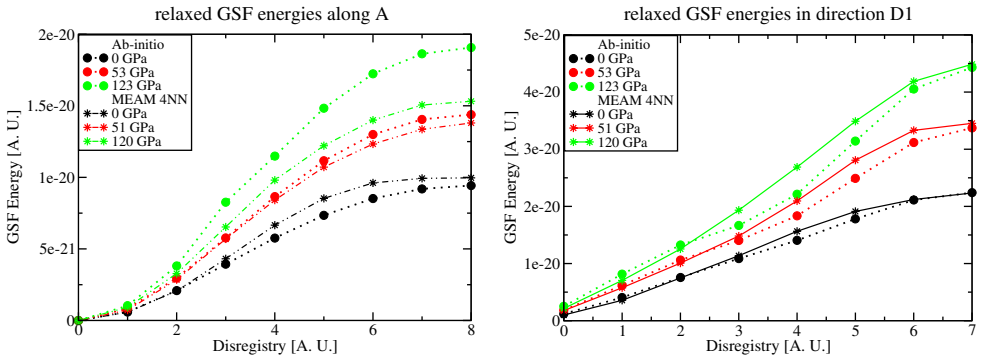

Figure 2. Comparison of the GSF energies along two axes— A and $D1$ (see figure 1)—obtained with our MEAM and *ab initio* calculations.

(This figure is in colour only in the electronic version)

Table 4. Vacancy formation energies.

Lat. param. (Å)	E_v^{rel} (eV)	E_v^{unrel} (eV)	E_v^{unrel} (eV) from [41]
3.303	2.67	3.139	3.25
3.28	2.143	2.568	3.07
3.18	−0.27	0.279	2.29
3.08	−2.889	−2.075	1.22
2.98	−5.955	−4.581	−0.21
2.88	−10.184	−7.324	−2.12
2.78	−15.082	−10.497	NA

4.3. Transferability evaluation

As is usual in such cases, we have computed other physical quantities to assess our potential parameters.

Our first task was to see whether this potential is dynamically stable. Therefore we tried to get the melting temperature of tantalum described by our model. The melted interface method [40] yields a melting temperature which is about 3700 K, while the experimental value is about 3290 K. This is satisfactory for a model which does not include any temperature data at all. More encouraging than this agreement is the fact that upon solidification, the melted part of the crystal recovers a BCC phase which is the only known stable phase for tantalum.

Second, using equation (18) we have computed relaxed and unrelaxed vacancy formation energies in cells of 31 250 atoms and compared results with the *ab initio* computation of Mukherjee *et al* [41] (see table 4):

$$E_v = (E^{at}_{N-1} - E^{at}_0)(N-1). \tag{18}$$

While the low pressure values are reasonable, the vacancy formation energy becomes negative at too low a pressure (before 6% compression). This is mostly due to the high negative values for t_1 and t_2. This is also a clue which indicates that our model does not work so well at high pressures because this happens later (about 12% compression) in *ab initio* calculations.

Third, we have also computed some relaxed surface energies in directions $A = [100]$, $B = [110]$, $C = [111]/2$, and $D = [112]$. Values are shown in table 5. To be absolutely

Table 5. Surface energies.

Surface index	Calculation cell	(eV Å^{-2})	(J m^{-2})
[111]	8C × 4B × 3D	0.333	5.328
[110]	9B × 5C × 2D	0.297	4.757
[112]	8D × 6C × 4B	0.332	5.321
[100]	20A × 5A × 5A	0.288	4.628

Table 6. Comparison between *ab initio* and classical computations of tantalum phase properties.

	V_0 (Å^3/atom)		$E_0 - E_{\mathrm{BCC}}$	
Phase	Potential	Abinit	Potential	Abinit
A15	17.77	18.42	0.052	0.028
FCC	18.37	18.54	0.176	0.239

sure of the numbers we ran every calculation a second time with a halved size cell and we got the same result (less than 0.1% relative difference). The positive values are quite acceptable; they are clues about the stability of the BCC phase. Still, they are higher than expected. Experimental data from polycrystalline solids gave an energy of about 3.018 J m^{-2} [42].

Finally we compare the phase ordering with the *ab initio* calculations in table 6. To get the *ab initio* values we used an overconverged calculation (better than 10^{-5} Hartree). The agreement between our model and *ab initio* results here is really surprisingly good. Even the equilibrium volume of an FCC phase is reproduced.

5. Results on dislocations and conclusions

The first test of our MEAM model was on edge dislocation simulations. They glide at a measurable rate when subjected to shears under 0.06%. This corresponds to a very low critical stress and is in good agreement with observations for BCC metals.

A second real life test of the potential was the study of screw dislocation stability. After introducing the elastic displacement field of a quadrupolar area of dislocations and a kinetic energy corresponding to 1800 K according to equation (19), we have relaxed the cell with a viscous damping algorithm down to a few tens of kelvins with the Beeler algorithm.

$$\tfrac{1}{2}m\sum_{i=0}^{N} v_i^2 = \tfrac{3}{2}Nk_{\mathrm{B}}T \tag{19}$$

Both hard core and easy core dislocations are stable. The core energy is about 1 eV/b which is in between results obtained by Woodward *et al* (0.9 eV/b) [15] and Wang *et al* (1.4 eV/b) [43]. The relative difference between them is about 0.003 eV/b which is not significant in view of the accuracy of any empirical potential. That is why we consider both core configurations in the following. The relaxed cores obtained are small with no significant partial extension.

Actually most studies of dislocations [43, 15, 14] use a pure energy minimization scheme to evaluate Peierls stress. Yet it is an important matter to know how exactly the Peierls stress should be computed: during movement, dislocations might follow a path of minimal energy for each atom or some local minima in the path may exist. In the first case a regular minimization might be used to compute Peierls stress: under stress above the critical one, atoms should move without obstacle and then an energy minimization scheme is sufficient for seeing dislocations gliding from each site to the next at the Peierls stress. In the second

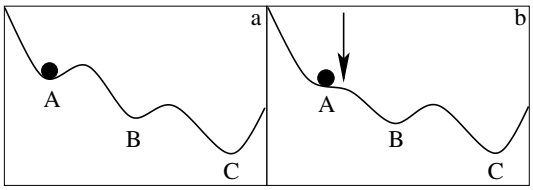

Figure 3. A ball in a simple potential energy landscape.

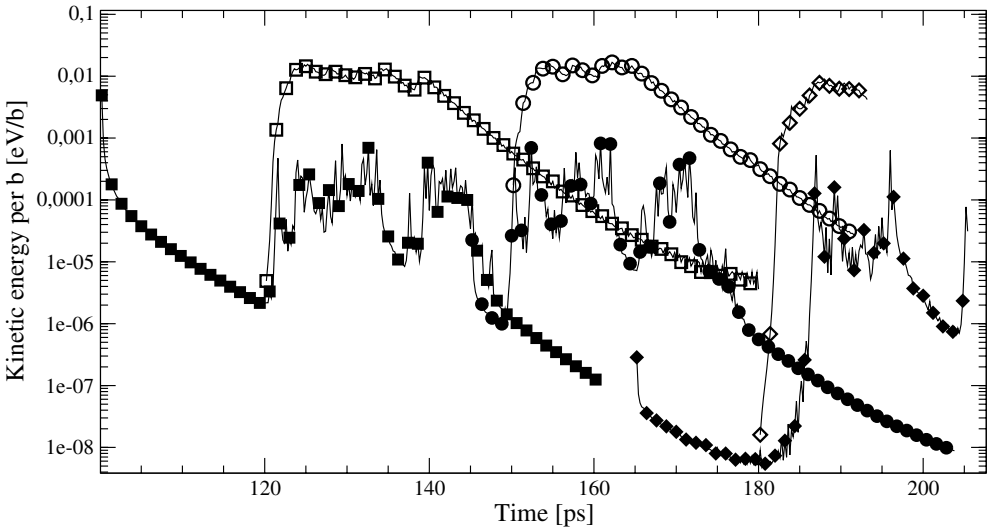

Figure 4. Evolution of the kinetic energy in the cell after application of a homogeneous displacement field to reach the first critical stress. Curves with square symbols represent the evolution of the kinetic energy when the plastic deformation is strong enough for immediately reaching the Peierls stress, that is to say +0.7%, while the increment of the elastic deformation is respectively +0.05% and +0.005% for the simulations plotted with circles and diamonds. Curves with open symbols stand for simulations with free dislocation cores, while their counterparts shown with filled symbols are the results obtained under Beeler's minimization.

case some true molecular dynamics might be required: the kinetics of the atoms in the core of dislocations may be important and must be described accurately when the Peierls stress is reached, because otherwise atoms could stay in some unnatural configurations. This point might be understood with the example of a ball rolling in a potential landscape as illustrated in figure 3. When the bump between valleys A and B is removed (parts (a) and (b)) the ball starts rolling. Under natural dynamics it is able to reach C while under minimization it will reach, then stay in state B. Obviously this scheme is oversimplified. During the movement of a dislocation there is some dispersion and the energy landscape seen by atoms of the dislocation core is strongly dependent on the position of the dislocation.

To address this problem we have made two kinds of calculations. In the first one we are using Beeler's algorithm on every atom in the simulation cell. At a critical stress, atoms begin to move and the kinetic energy in the simulation cell increases suddenly. This is shown in figure 4 by the curves with filled symbols. Curves start when a homogeneous displacement field is applied to the cell. After a few picoseconds of relaxation, the kinetic energy of the simulation cell increases suddenly because atoms in the core of the dislocations are moving. Though those atoms get reorganized, dislocations are not able to cross the Peierls barrier. It is necessary to

keep increasing the stress to get a real movement of the dislocations. Then under minimization we get two critical stresses: a first one corresponding to dislocation reorganization and a second one which seems to be the Peierls stress.

For both hard and easy core dislocations, and with a maximum critical resolved shear stress in a [110] plane (that is to say the dislocations should move in direction $\langle 112 \rangle$), the critical strain obtained in this way (full minimization of energy) is between 1.5% and 1.8%. That is a Peierls stress about or above 1 GPa. The core reorganization happens at strains of about 0.7% and 1.2% depending on whether the dislocations are hard core or easy core.

This two-step (with two critical stresses) movement process is suspect and must be checked because of the very sudden increase of the kinetic energy.

The first idea is to check whether it is the result of the large step used for application of the strain. Then we decreased the size of the step down to 0.005%. For the extreme right curve in figure 4 this means that nothing special happens in the simulation cell under a pure shear strain of 0.660% and that even the very small increase of deformation which leads to a shear of 0.665% is enough to result in some very big displacements of the atoms in the cores of dislocations. The strong similarity between curves resulting from steps of 0.7%, 0.05% and 0.005% tells us that the phenomenon does not depend on the increment. We conclude that at the first critical stress an energy barrier is crossed and this results in a cascade of atom movements.

It becomes obvious that the real kinetics of this event must be taken into account. For this we have defined an elastic region distant from the dislocation cores by 6 b. In this region we keep using the Beeler algorithm. Meanwhile, in the core regions, the standard Verlet algorithm is used. With these free cores, when the first critical stress is reached, dislocations are moving. The evolution of the kinetic energy is displayed by the curves with open symbols in figure 4.

This calculations underline the importance of using a realistic atom dynamics in computation of the Peierls stress. The new resulting Peierls stresses are the following: for easy core dislocations, about 760 MPa and for hard core ones, about 450 MPa.

We have computed the Peierls stress of a screw dislocation at various pressures with this potential. Under pressure above 10–20 GPa, the screw dislocations show a tendency to glide in the [112] plane, even if the maximally resolved shear stress is in a [110] plane. As we have not extensively sampled the GSF in the [112] plane in our force field, we cannot tell whether this is a correct behaviour or not. Doing so would at least require partial sampling of the [112] energy surface.

We can sum up our conclusions in the following way.

First, an empirical potential based exclusively on elastic properties and Γ-surfaces appears to be able to accurately describe homogeneous dislocation slip in the crystal lattice. This is in good agreement with the Peierls–Nabarro model. This is only apparently in disagreement with the Wang *et al* conclusion [43] about the effect of the GSF on dislocations, because they have considered only the unstable stacking fault and the Γ-line reaching it, while we have considered the full surface and in particular the part associated with the low disregistry vectors which is supposed to be responsible for the shape of the dislocation core. It may be noticeable that the resulting Peierls stress for hard core screw dislocations is closer to the experimental one than that computed with another method. However, this is just a hint of the potential importance of hard core dislocation. Indeed, as noticed previously, there may be some other mechanisms resulting in the discrepancy with experiment and, to our knowledge, the importance of hard core dislocations has not been seen in any other work. The reason for this might be the mere fact that in every other study, cores of dislocations are relaxed from the elastic displacement field with a strong minimization algorithm like the generalized gradient one, which falls in the closest local minimum, while we use some real annealing.

Second, we have shown that the MEAM formalism is able to describe correctly Γ-surfaces. With only a few parameters we have been able to reproduce a large set of properties.

Third, extension of the MEAM formalism to 4th nn is very important if one wishes to reproduce properties like the high degree of elasticity (i.e. evolution of elastic properties under large stress) both because of the importance of the symmetries of the neighbour shells and because of the high coordination numbers from 3rd nn and 4th nn in BCC. Still, extension in range of the MEAM is essential to get some more than local—in the phase space—agreement with *ab initio* calculations: with a short range potential, one might succeed in reproducing many properties of the bulk, even a substantially distorted one, but configurations like the ones we have used for evaluating force ranges can be described neither accurately nor approximately. Thus we can guess that the agreement between the potential and the data set used for the fit is local, just as Laio *et al* did in [44]; there are some strong discrepancies between the model and reality as shown in our examples if the potential range is not long enough.

Fourth, we must underline the importance of using a technique including a natural dynamics of atoms in the core of dislocations during the gliding process. To our knowledge, this study is the first to test such a technique and our results show it to have a very large impact.

Finally, there are good hopes that, with more data (e.g. on other Γ-surfaces, especially [112]), an improved formalism—in particular for the ρ and $\bar{\rho}$ functions and the angular screening—for the MEAM potential, we might succeed in providing predictions for a lot of properties of microstructural defects in materials like tantalum for which EAM force fields have failed. With such data it would at least be possible to probe the known gliding mechanism of screw dislocations (twinning and anti-twinning) with a satisfactory reliability. Yet this kind of sampling was not within our reach, due to the very high complexity of the [112] surface in BCC crystals.

Acknowledgments

The authors would like to acknowledge valuable discussions with Dr C Denoual, Dr F Jollet, Dr R Madec, Dr Y-P Pellegrini and C Bercegeay which oriented this work and helped its progress. Also, we would like to thank B Magne for his kind and efficient support in developing Stamp, the CMD code that we have used and developed for this work.

References

[1] Bourasseau E, Haboudou M, Boutin A, Fuchs A and Ungere P 2003 *J. Chem. Phys.* **118** 3020–34
[2] Croixmarie V 2004 Étude du changement de structure de la prp^C murine par simulation de dynamique moléculaire—modélisation de fibres peptidiques *PhD Thesis* University of Orsay—Paris XI
[3] Jomard G 2004 *CIMTEC Proc.* A vol 42
[4] Maillet J-B, Mareschal M, Soulard L, Ravelo R, Lomdahl P, Germann T and Holian B L 2001 *Phys. Rev.* E **63** 016121
[5] Germann T, Tanguy D, Holian B L, Lomdahl P, Mareschal M and Ravelo R 2004 not yet published
[6] Basinski Z, Duesberry M and Taylor R 1971 *Can. J. Phys.* **49** 2160
[7] Marian J, Cai W and Bulatov V 2004 *Nat. Mater.* **3** 158
[8] Daw M, Foiles S and Baskes M 1993 The embedded atom method: a review of theory and applications *Materials Science Reports* vol 9 (Amsterdam: Elsevier) pp 251–310
[9] Strachan A, Çağin T, Gülseren O, Mukherjee S, Cohen R and Goddard W III 2004 *Modelling Simul. Mater. Sci. Eng.* **12** S445–59
[10] Takeuchi S and Maeda K 1977 *Acta Metall.* **25** 1485
[11] Suzuki T, Kamimura Y and Kirchner H 1999 *Phil. Mag.* A **79** 1629–42
[12] Segall D, Arias T, Strachan A and Goddard W III 2001 *Preprint* cond-mat/0103084
[13] Moriarty J, Belak J, Rudd R, Söderlind P, Streitz F and Yang L 2002 *J. Phys.: Condens. Matter* **14** 2825–57

[14] Yang L, Söderlind P and Moriarty J 2001 *Phil. Mag.* A **81** 1355
[15] Woodward C and Rao S 2002 *Phys. Rev. Lett.* **88** 216402
[16] Vitek V 1968 *Phil. Mag.* **18** 773
[17] Khotari M and Anand L 1998 *J. Mech. Phys. Solid* **46** 51–67
[18] Cai W, Bulatov V, Chang J, Li J and Yip S 2001 *Phys. Rev. Lett.* **86** 5727
[19] Ismail-Beigi S and Arias T 2000 *Phys. Rev. Lett.* **84** 1499
[20] Rao S, Hernandez C, Simmons J and Woodward C 1998 *Phil. Mag.* A **77** 231
[21] Baskes M 1992 *Phys. Rev.* B **46** 2727
[22] Li Y, Siegel D, Adams J and Liu X-Y 2003 *Phys. Rev.* B **67** 125101
[23] Baskes M 1989 *Phys. Rev.* B **49** 2727
[24] Rose J, Smith J, Guinea F and Ferrante J 1984 *Phys. Rev.* B **29** 2963–9
[25] van Beurden P and Kramer G 2001 *Phys. Rev.* B **63** 165106
[26] Lee B-J, Baskes M, Kim H and Choo Y 2001 *Phys. Rev.* B **64** 184102
[27] Chen N X 1990 *Phys. Rev. Lett.* **64** 1193
[28] Joós B and Duesberry M 1997 *Phys. Rev. Lett.* **78** 266
[29] Lu G, Bulatov V and Kaxiras E 1999 *Preprint* cond-mat/9907352
[30] Schmid E and Boas W 1928 *Kristallplastizität* (Berlin: Springer)
[31] Bernard S 2001 private communication
[32] Blaha P, Schwarz K and Sorantin P, *Wien: A Full-Potential, Linearized Augmented Plane Wave Package of Programs for Crystals* Institut für Technische Elektrochemie, Technische Universität Wien
[33] Perdew J, Chevary J, Vosko S, Jackson K, Pederson M, Singh D and Fiolhais C 1992 *Phys. Rev.* B **46** 6671
[34] *The Abinit Code* published under the gnu/gpl license, is a common project of the Université Catholique de Louvain, Corning incorporated, the Université de Liège, the Commissariat à l'Énergie Atomique, Mitsubishi Chemical corp., and other contributors (http://www.abinit.org)
[35] Gonze X, Beuken J, Caracas R, Detraux F, Fuchs M, Rignanese G, Sindic L, Verstraete M, Zérah G, Jollet F, Torrent M, Roy A, Mikami M, Ghosez P, Raty J and Allan D 2002 *Comput. Mater. Sci.* **25** 478–92
[36] Hartwigsen C, Goedecker S and Hutter J 1998 *Phys. Rev.* B **58** 3641
[37] Perdew J, Burke K and Ernzerhof M 1996 *Phys. Rev. Lett.* **77** 3865
[38] Beckstein O, Klepeis J, Hart G and Pankratov O 2001 *Phys. Rev.* B **63** 134112
[39] Mehl M, Klein B and Papaconstantopoulos D 1995 *Intermetallic Compounds: Principles and Practice* vol 1 *Principles* ed J Westbrook and R Fleisher (New York: Wiley) pp 195–210
[40] Tomagini O, Ercolessi F, Iarlori S, Tolla F D and Tosatti E 1996 *Phys. Rev. Lett.* **76** 1118
[41] Mukherjee S, Cohen R and Gülseren O 2003 *J. Phys.: Condens. Matter* **15** 855–61
[42] Mezey L and Giber J 1982 *Japan. J. Appl. Phys.* **21** 1569
[43] Wang G, Strachan A, Çağin T and Goddard W III 2003 *Phys. Rev.* B **67** 140101
[44] Laio A, Bernard S, Chiarotti G, Scandolo S and Tosatti E 2000 *Science* **287** 1027